ResearchGate

See discussions, stats, and author profiles for this publication at: https://www.researchgate.net/publication/361378854

White Light Correlation Holography Using a Random Lens for Astronomical Imaging Applications

Conference Paper · April 2022

DOI: 10.1109/PIERS55526.2022.9792955

CITATIONS
0

READS
72

4 authors, including:

Vijayakumar Anand
University of Tartu
217 PUBLICATIONS **2,520** CITATIONS
SEE PROFILE

Tomas Katkus
Swinburne University of Technology
110 PUBLICATIONS **1,037** CITATIONS
SEE PROFILE

Saulius Juodkazis
Swinburne University of Technology
1,026 PUBLICATIONS **25,951** CITATIONS
SEE PROFILE

All content following this page was uploaded by Vijayakumar Anand on 20 June 2022.

The user has requested enhancement of the downloaded file.

White Light Correlation Holography Using a Random Lens for Astronomical Imaging Applications

V. Anand[1], **S. H. Ng**[1], **T. Katkus**[1], **and S. Juodkazis**[1, 2]

[1]Optical Sciences Centre and ARC Training Centre in Surface Engineering for Advanced Materials (SEAM)
School of Science, Swinburne University of Technology, Hawthorn, VIC 3122, Australia
[2]Tokyo Tech World Research Hub Initiative (WRHI), School of Materials and Chemical Technology
Tokyo Institute of Technology, 2-12-1, Ookayama, Meguro-ku, Tokyo 152-8550, Japan

2022 Photonics & Electromagnetics Research Symposium (PIERS) | 978-1-6654-6023-1/22/$31.00 ©2022 IEEE | DOI: 10.1109/PIERS55526.2022.9792955

Abstract— Holography technologies (HOLOTECH) are attractive than lens-based direct imagers due to the capabilities of HOLOTECH to record and reconstruct complete three-dimensional information of an object or an event with one or a few camera shots. In the past, HOLOTECH was mainly associated with coherent light and as a matter of fact, the development and application of HOLOTECH waited several years until the invention of laser even though the idea of holography was introduced much earlier. As the initial HOLOTECH concepts were based on two-beam interference, the lack of spatial and temporal coherence in incoherent light introduced numerous challenges and demanded stringent optical configuration requirements. For this reason, HOLOTECH was mostly applied with coherent light sources and for the "light in/from space" which is spatially and temporally incoherent, HOLOTECH could not be applied efficiently for three-dimensional imaging. In the recent years, there has been a transformation in the concepts of HOLOTECH which is rapidly reshaping the field of incoherent imaging. The invention of interferenceless coded aperture correlation holography (I-COACH) has rekindled the area of spatially incoherent holography and the two-beam interference is no longer a requirement to record and reconstruct three-dimensional information. I-COACH concept was adapted into satellite telescope applications as partial aperture imaging technique and synthetic aperture imaging method. Both have proven to perform better than lens-based imagers under extreme imaging conditions. In this study, we extend the concept of I-COACH to a land-based telescope. This concept is called as 3D telescope with sparse coded apertures (3D-TELESCA). The 3D-TELESCA concept consists of quasi-random coded apertures with different sizes that are sparsely distributed within the aperture. Every coded aperture consists of two phase functions: quadratic and linear to generate carrier waves to deliver the intensity distribution to the sensor within the sensor area. The linear and quadratic phase depends upon the radius vector of the coded aperture to the center of the sensor. This aperture consists of circular zones capable of rotating about the center independently of one another. The above rotation enables multiple aperture configurations that can generate intensity distributions with cross-correlation significantly lower than autocorrelation which is desirable for statistical averaging. The imaging process consists of four steps: PSF training, PSF engineering, recording and reconstruction in which the first two are one-time offline procedure and the next two are online procedures and so only the final two steps impact the temporal resolution of the system. In the first step, a pinhole is scanned axially, and the corresponding PSF intensity distributions are recorded and saved as a library. The PSF library is engineered using phase-retrieval algorithms and computationally processed to reduce background noise. For imaging application, an object is mounted, and the object intensity (OI) distribution is recorded under identical conditions of optical configuration for recording PSF library. The OI is processed with the engineered and processed PSF library and the 3D image of the object is reconstructed. The developed method can be applied directly to "light in/from space" for three-dimensional imaging in regular as well as synthetic aperture based astronomical imaging systems. Preliminary experimental results are presented using a single element of the 3D-TELESCA.

1. INTRODUCTION

Imaging systems have unique requirements of illumination, photon budget, numerical aperture, field of view, lateral and axial resolutions, etc., depending upon the area of application. Astronomical imaging methods unlike microscopy are required to work with self-luminous objects where the object illumination is not within our control [1]. Since the light received from space is weak, it is necessary to collect all the available light and extract useful information from it. In principle, a reflective lens with a large diameter and no chromatic aberration is the ideal imaging component for this. However, most of the reflective telescopes such as Cassegrain type telescope block most of the central part of the incoming light as shown in Fig. 1 [2]. This has two effects. The first is the loss of intensity which is not desirable and secondly, the block in the central part results in an

Authorized licensed use limited to: University of Tartu Estonia. Downloaded on June 20,2022 at 09:35:35 UTC from IEEE Xplore. Restrictions apply.

annular type aperture which results in an increase in sidelobes and consequently distorts the image. The distance between the primary mirror with diameter D and the sensor is $z_1 + z_2 + z_3$. The ratio of the annular aperture is defined as R = width of annulus/radius of aperture. The point spread functions (PSFs), the modulation transfer functions (MTFs), where MTF = $|\mathfrak{F}(\text{PSF})|$, where F is the Fourier transform operation, and images of a test object 'PIERS 2021' for different ratio of the annular aperture are shown in Fig. 2 [3]. The test object was designed in font style Calibri with a font size variation is shown in Fig. 2(a). The images of PSF, MTF and images of the test object are shown in Fig. 2(b). As the width of the annular aperture decreases, the higher spatial frequencies are attenuated more which results in the loss of resolution which is seen in the images of the test object [2].

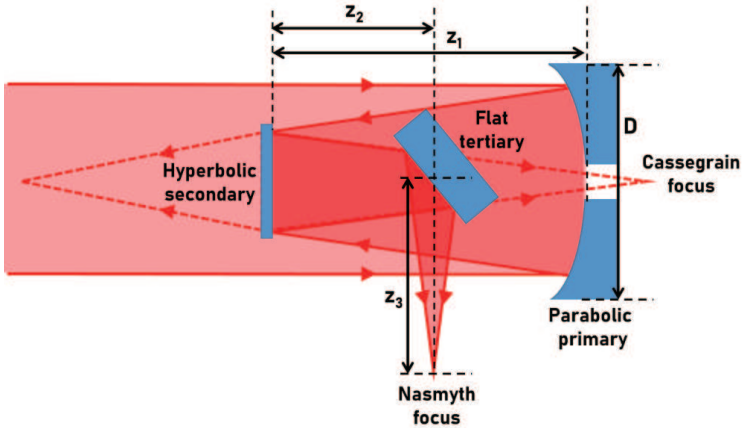

Figure 1: Optical configuration of Cassegrain telescope. The blocking of the central part of light by hyperbolic secondary and flat tertiary is seen.

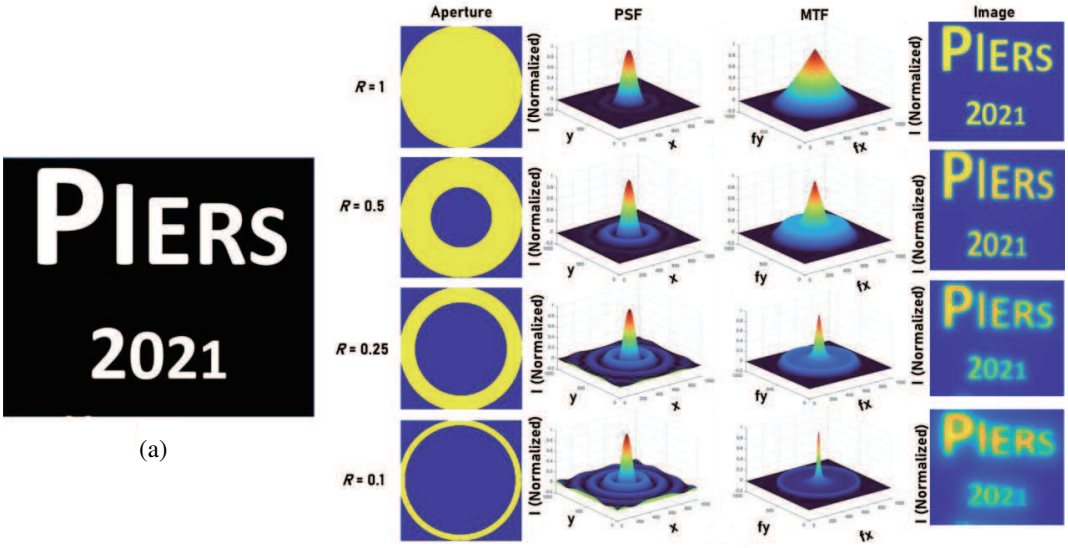

Figure 2: (a) Test object. (b) Images of the apertures, PSF, MTF and image of the test object for different values of ratio R-1, 0.5, 0.25 and 0.1.

Recently, a coded aperture method called partial aperture imaging system (PAIS) was proposed to solve this problem [4]. In this approach, the annular aperture configuration was retained but the implementation was on a satellite telescope model. This approach considers synchronously orbiting satellites acting as a temporal coded aperture and another satellite as sensor respectively. The orbiting satellites generate a temporal annular coded aperture that introduces random modulation along with a carrier wave which transfers the controlled scattered intensity to the sensor. A statistical averaging method was used to boost the higher spatial frequencies. This method was able to

Authorized licensed use limited to: University of Tartu Estonia. Downloaded on June 20,2022 at 09:35:35 UTC from IEEE Xplore. Restrictions apply.

image objects with the same resolution as the full aperture by averaging over 63 images per scene with multiple coded phase masks. Experimentally the method was able to retain the resolution until R $\sim$ 0.1. Later this method was adapted to synthetic aperture imaging method [5]. Recently, modified approaches were proposed and demonstrated to enhance the signal to noise ratio [6, 7]. While the above approaches are attractive and can improve the resolution of imaging system significantly, there are many drawbacks. The formation of temporal coded aperture may not be suitable for recording dynamic objects. The power efficiency of the system is only one-hundredth of the case with full aperture. Another most important factor is the spectral width. All the above studies have been demonstrated using spatially incoherent but temporally coherent light sources. However, the light from space is both spatially as well as temporally incoherent. In this manuscript, we propose a radical approach to solve all the above problems with preliminary results. The study proposes to transform a Cassegrain telescope into a 3D telescope with sparse coded aperture (3D-TELESCA) based on interferenceless coded aperture correlation holography (I-COACH) [8]. The manuscript consists of five sections. In the next section, the optical configuration of 3D-TELESCA and methodology is presented. The design and fabrication of a sub-modulator is presented in the third section. The preliminary experimental results are presented in the fourth section. The conclusion and future perspectives are presented in the final section.

2. METHODS

The optical configuration and concept of 3D-TELESCA is shown in Fig. 3. This optical configuration has been considered based on the recent revolution in fabrication technologies [9], PAIS [4–7] and interesting concepts on diffractive telescopes [10, 11]. The aperture consists of circular rotatable zones and within the circular zones, mutually exclusive coded aperture sub-modulators with cross-correlation significantly lower than autocorrelation are installed. There is only one degree of freedom online i.e., rotation of the circular zones as shown in Fig. 3. The imaging concept of 3D-TELESCA consists of four steps: design of coded aperture sub-modulator, coded aperture architectures to generate mutually exclusive events, record PSF library and synthesize edge enhanced PSF library, image an astronomical object and reconstruct the object using recorded and synthetic PSF library and computational processing.

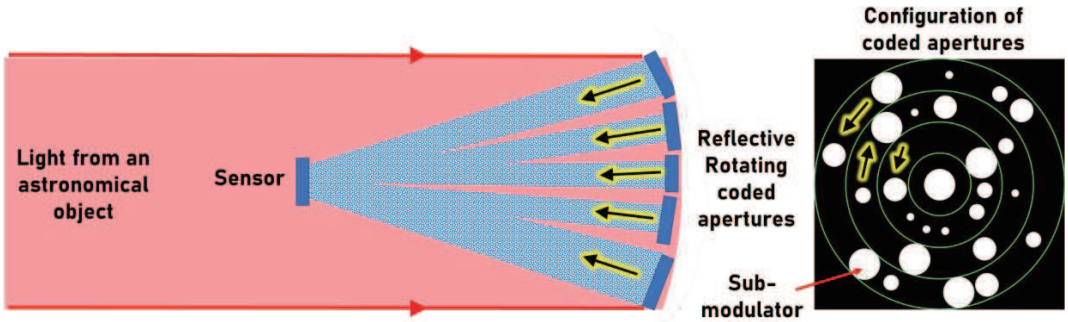

Figure 3: Optical configuration and concept of 3D-TELESCA. The green boundaries indicate the zones, and each zone can rotate independently of another along the axis. A sub-modulator is indicated.

2.1. Design of Coded Aperture Architectures

The coded aperture sub-modulators' phase distributions are calculated using Gerchberg-Saxton algorithm (GSA) as shown in Fig. 3 [12]. Every sub-modulator of the 3D-TELESCA must be designed separately and carrier waves consisting of quadratic and linear phases must be introduced depending upon the radius vectors. Since the circular motion of the sub-modulators introduces only a change in azimuthal angle and the distance between the aperture and sensor is constant, the linear and quadratic phase factors requirement remain independent of the rotation.

A matrix consisting of a single sub-modulator was used as the input amplitude matrix and a random phase was used as the input phase. The resulting complex amplitude is Fourier transformed and the resulting complex amplitude's phase is retained. An amplitude constraint is applied depending upon the sensor area and the distance between the sensor and coded aperture. The resulting complex amplitude is inverse Fourier transformed. This process is iterated until a solution is obtained. Light from a distant object is modulated by the sub-modulators and the modulated light

Authorized licensed use limited to: University of Tartu Estonia. Downloaded on June 20,2022 at 09:35:35 UTC from IEEE Xplore. Restrictions apply.

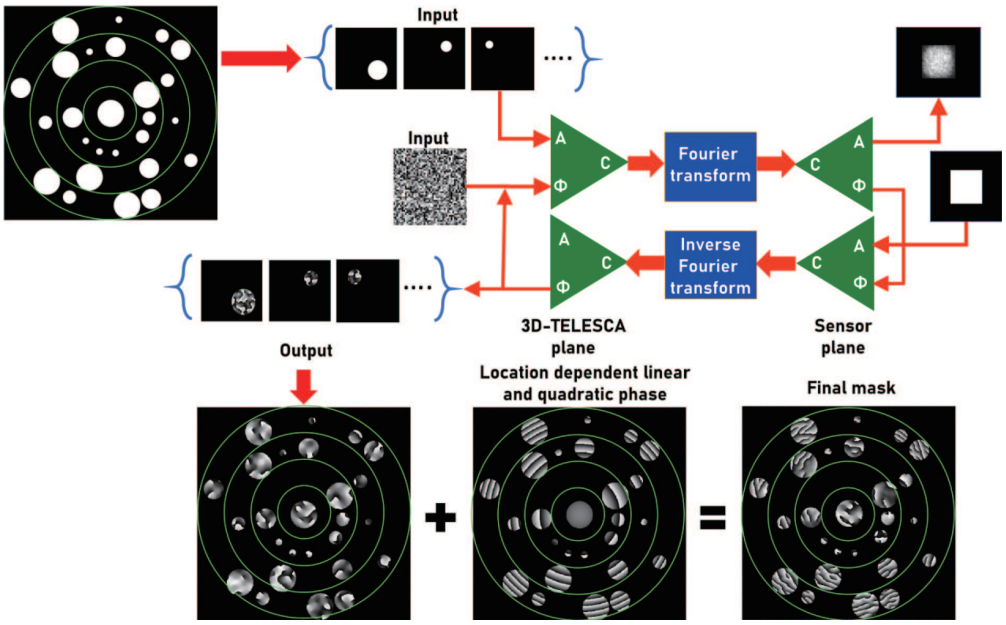

Figure 4: Implementation of GSA for designing the coded apertures of 3D-TELESCA.

is delivered to the sensor with a distribution within the sensor area by the carrier waves generated by the linear and quadratic phase factors. In the next step, the locations of the sub-modulators were optimized to generate mutually exclusive intensity distributions i.e., the cross-correlation values are insignificant compared to the autocorrelation values.

2.2. Synthesis of Mutually Exclusive Coded Aperture Architectures

In the previous studies, active light modulators were used for statistical averaging. In this study, the statistical averaging is achieved by changing the architectures of the coded apertures in time. To have noise reduction by statistical averaging, the cross-correlation between two intensity distributions must be as low as possible [13]. A search algorithm was used to calculate the coded aperture architectures that will generate intensity distributions with low cross-correlation values. The angle search algorithm is shown in Fig. 5. The algorithm begins with an initial coded aperture architecture and creates a copy of this architecture. In the copied version, the nth zone was rotated by an angle Φ. A Fresnel transform was calculated for the original and the rotated version and the resulting intensity distributions were cross-correlated. If the cross-correlation value at $(x = y = 0)$ is smaller then the angle is increased by Φ and the process is repeated until the minimum value was

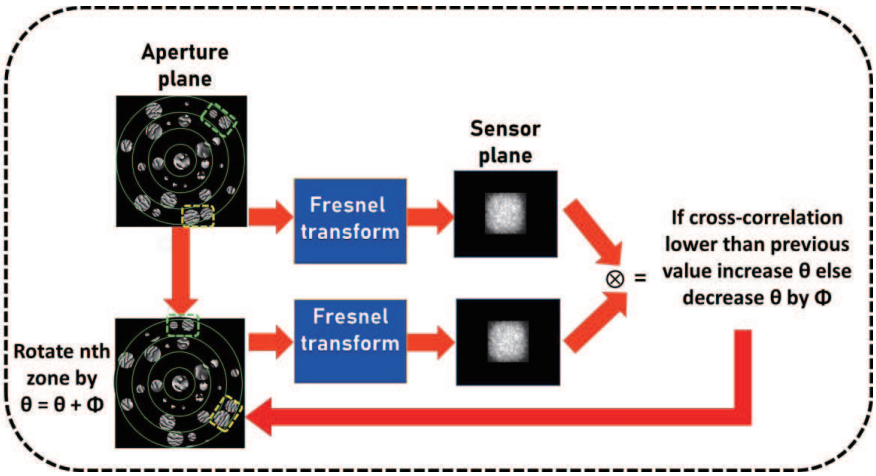

Figure 5: Search algorithm for generating coded aperture architectures. The green and yellow dotted lines show the rotated zone (40 degrees) and the symbol $\otimes$ indicates a 2D correlation operation.

Authorized licensed use limited to: University of Tartu Estonia. Downloaded on June 20,2022 at 09:35:35 UTC from IEEE Xplore. Restrictions apply.

obtained. If the cross-correlation value increases, then the change in angle is undone and rotated in the opposite direction. This process is then repeated for other zones.

2.3. Regular and Edge Enhanced PSF Library

In the next step, the PSF library is recorded by arranging the sub-modulators at different optical architectures generated in step-2. Four nearly mutually exclusive architectures of coded apertures, the corresponding PSF distributions are shown in Fig. 6(a). The images obtained for the same test object for the four cases and the reconstructed intensity distributions are shown in Fig. 6(a). The statistically averaged result of the four cases shown in Fig. 6(b) indicates the enhancement in signal to noise ratio. This is a linear optical system and so the image intensity I_O obtained for an object O is given as $I_{PSF} \otimes O$, where '$\otimes$' is a 2D convolution operator. The reconstruction is achieved by a cross-correlation given as $I_O * I_{PSF}$ where '*' is the 2D correlation operator. This regular correlation is also called as matched filter. In this reconstruction, a phase-only filter was used to reduce the background noise [13]. From the results, it is seen that the statistical averaging improved the results but still suffer from low signal to noise ratio. The plot of the autocorrelation and cross correlation of the four cases are shown in Fig. 6(c). The maximum values were obtained for autocorrelation and the minimum values were obtained for cross-correlation.

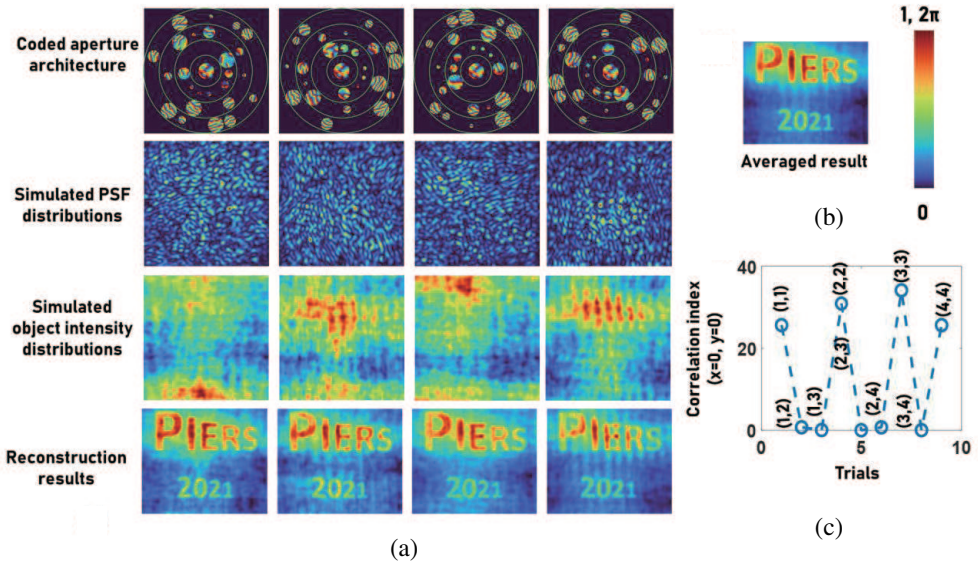

Figure 6: Images of different coded aperture architecture, simulated intensity distribution, reconstruction results and averaged reconstruction results. The plot of correlation index measured at the origin ($x = 0$, $y = 0$) for cross-correlation and autocorrelation operations for the four cases. The values (a,b) in (c) indicate the case numbers that were correlated.

In many incoherent imaging methods such as Fresnel incoherent correlation holography (FINCH), the edge enhancement was achieved using a vortex filter [14, 15]. In FINCH, an object wave is split into two and modulated by quadratic phase masks with different focal lengths and interfered to create the hologram. The image reconstruction is carried out using a numerical Fresnel back propagation. For edge enhancement, one of the beams was modulated by a multifunctional diffractive element made up by modulo-2π phase addition of quadratic phase mask and spiral phase mask. During numerical backpropagation, edge enhanced images of the objects are obtained. Unlike FINCH, coded aperture methods do not require two beam interference which does not give an opportunity to introduce an edge enhancement like FINCH. Recent studies indicated that the correlation-based approach renders a uniform behavior irrespective of the presence of a vortex filter [16]. Recently, an edge enhancement technique was developed for coded aperture imaging methods using a phase-retrieval algorithm [17]. During the edge enhancement study, it was noticed that if the edge enhanced reconstructions were subtracted from the regular reconstructions, a contrast enhancement in addition to significant reduction in background noise was noticed. The schematic of the phase retrieval algorithm for synthesizing the edge enhanced PSF is shown in Fig. 7(a). For simplicity, the Fourier transform of the synthetic PSF is assumed to be pure phase function, i.e., amplitude is constant, but phase varies. The complex conjugate of the Fourier trans-

Authorized licensed use limited to: University of Tartu Estonia. Downloaded on June 20,2022 at 09:35:35 UTC from IEEE Xplore. Restrictions apply.

form of the recorded PSF is multiplied with an initial guess pure phase function and the result is Fourier transformed. The resulting complex amplitude's magnitude is replaced by a donut shaped intensity distribution (I_D) while the phase is retained. This donut shaped intensity is generated by diffracting light by a spiral phase plate [15]. The new complex amplitude at plane P_1 is inverse Fourier transformed and inverse of the conjugate of the Fourier transform of the PSF is multiplied to the result. The result is converted into a pure phase function again at plane P_2. This process is iterated until an optimal solution is obtained. The edge enhanced image of the test object is shown in Fig. 7(b). The contrast enhanced image without reduced background noise is shown in Fig. 7(c). The averaged result is shown in Fig. 7(d). Comparing the results with the previous approach, the contrast enhancement method improved the sharpness and rendered a background with a uniform noise.

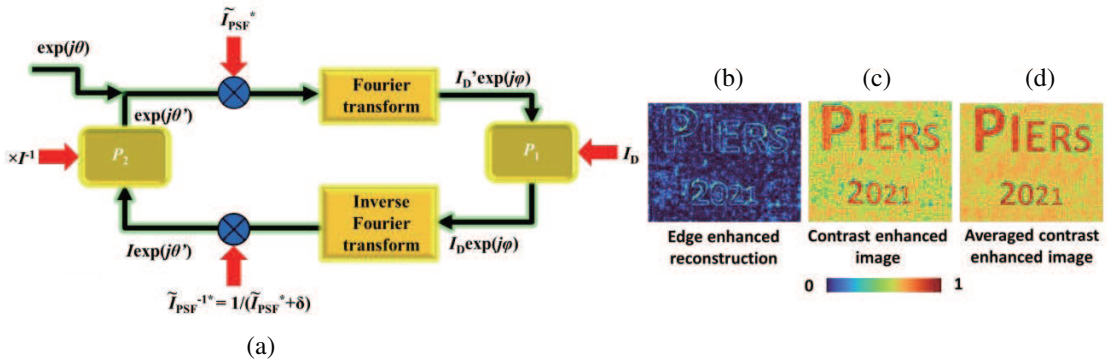

Figure 7: (a) Schematic of the phase-retrieval algorithm for edge enhancement. (b) Edge enhanced reconstruction. (c) Contrast enhanced imaging. (d) Averaged contrast enhanced image.

3. DESIGN AND FABRICATION OF A CODED APERTURE SUB-MODULATOR

A preliminary study was carried out by designing and fabricating a single coded aperture sub-modulator. For simplicity, it is assumed that the sub-modulator lies at the center of the aperture and so there is only a quadratic phase involved and no linear phase. In principle, this sub-modulator is nothing but a quasi-random lens (QRL) [18]. A QRL behaves like a regular lens but instead of collecting the light to a point, it collects it to a predefined area and in this case, the predefined area is the sensor area. This is like causing controlled scattering as within the selected area light is scattered. The QRL was designed with a scattering ratio $\sigma = 0.12$ and a focal length of $f = 5$ cm and $2f$ configuration i.e., object distance and image distance are 10 cm. The modulo-2π phase addition procedure of the quasi-random phase generated by the GSA as shown in Fig. 4 and a quadratic phase with $f = 20$ cm is shown in Figs. 8(a)–8(d). For easier fabrication, the phase pattern was binarized to two phase levels (0, π). The QRL was designed for $\lambda = 600$ nm, diameter of 5 mm with a pixel size of 500 nm. This design was fabricated using electron beam lithography system (RAITH150$^{\text{TWO}}$). Polymethyl Methacrylate (PMMA) 950 K was spin coated on Indium-Tin-Oxide (ITO) coated glass substrates with a thickness of approximately 600 nm and baked. After baking some of the PMMA was removed to expose the ITO layer which was connected to the metal clip of the sample holder of electron beam system to provide a grounding path for the electrons. This procedure reduces the charging problem during fabrication. The electron beam system was operated at 10 kV acceleration voltage, 120 µm aperture, beam current ~ 3 nA, write field of 100 µm and working distance of 10 mm. The writing time was about 7 hours. The fabricated device was developed in Methyl Isobutyl Ketone (MIBK) and Iso-propyl Alcohol (IPA). The optical microscope image of the fabricated QRL is shown in Fig. 8(e).

4. OPTICAL EXPERIMENTS

The fabricated device was used for imaging experiments. The PSF was recorded using a point object with a diameter of 100 µm located at 10 cm from the QRL and an image sensor (Thorlabs DCU223M, 1024 pixels ×768 pixels, pixel size = 4.65 µm) was located at a distance of 10 cm from the QRL. The pinhole was critically illuminated using a red LED with $\lambda = 630$ nm and $\Delta\lambda \sim 10$ nm. The image of the red PSF is shown in Fig. 9(a). Then the red LED was replaced by a white light

Authorized licensed use limited to: University of Tartu Estonia. Downloaded on June 20,2022 at 09:35:35 UTC from IEEE Xplore. Restrictions apply.

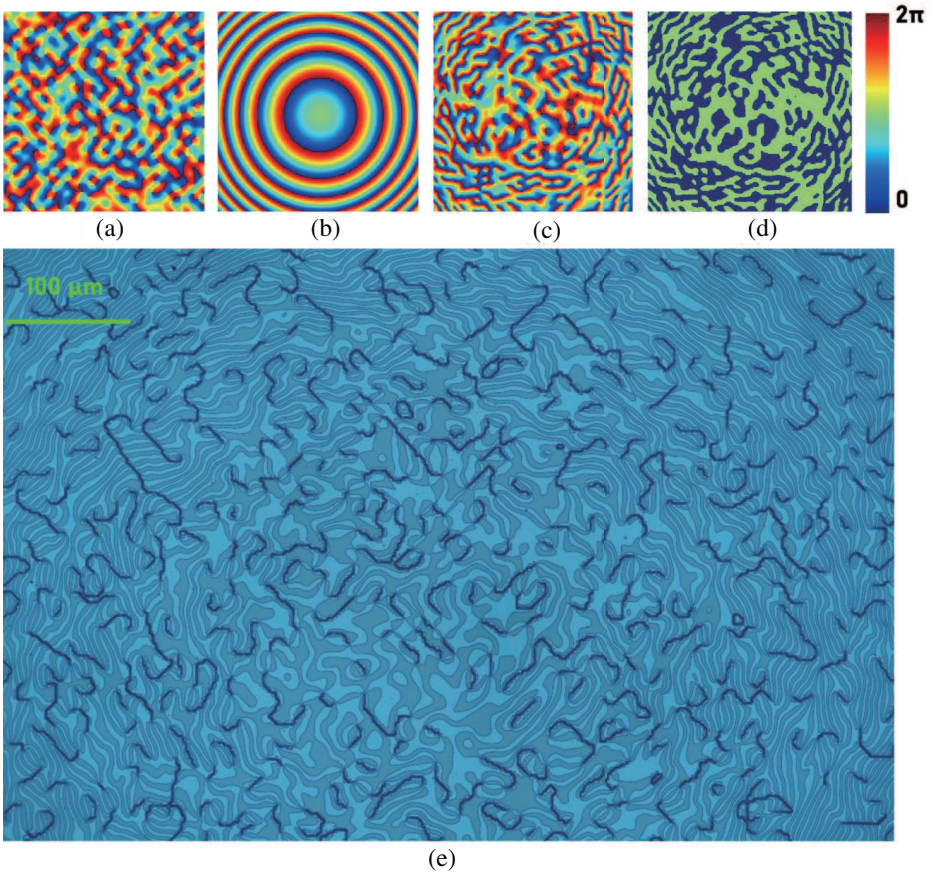

Figure 8: (a) Phase pattern generated from GSA with $\sigma = 0.12$, (b) Quadratic phase function with $f = 5\,\text{cm}$, (c) phase of QRL and (d) phase of binarized QRL. (e) Optical microscope image of the QRL fabricated by electron beam lithography.

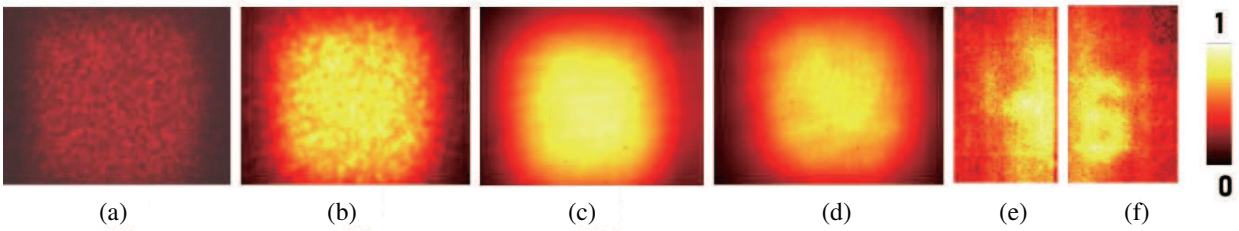

Figure 9: Images of (a) red PSF, (b) white PSF. Intensity distribution obtained for (c) number '4', (d) number '6'. Reconstruction results using non-linear reconstruction of (e) number '4' and (f) number '6'.

source (Fiber-Lite DC-950, Dolan-Jenner industries, Full width at half maximum $\Delta\lambda 270\,\text{nm}$) and the white PSF was recorded as shown in Fig. 9(b). Two objects namely number '4' and number '6' of the USAF resolution target were mounted one after the other at distances 10 cm and 10.6 cm and the intensity distributions were recorded as shown in Figs. 9(c) and 9(d) respectively. The reconstruction results using the non-linear correlation approach for the two objects are shown in Figs. 9(e) and 9(f) respectively [19]. Two approaches were tried here. For the number '6' a deep learning approach was tried using a pre-trained noise reduction network of the deep learning toolbox of MATLAB. Images of the number '6' was generated using different noises for training and 25 images from the training set is shown in Fig. 10(a). The noise removed image from the deep learning approach is shown in Fig. 10(b). The edge enhancement approach was applied to the number '4' and the noise removal by subtracting the edge enhanced reconstruction from the result of non-linear reconstruction is shown in Fig. 10(c). By comparing Figs. 10(b) and 10(c), it seems that both approaches have potential to reduce noise in the reconstructed images.

Authorized licensed use limited to: University of Tartu Estonia. Downloaded on June 20,2022 at 09:35:35 UTC from IEEE Xplore. Restrictions apply.

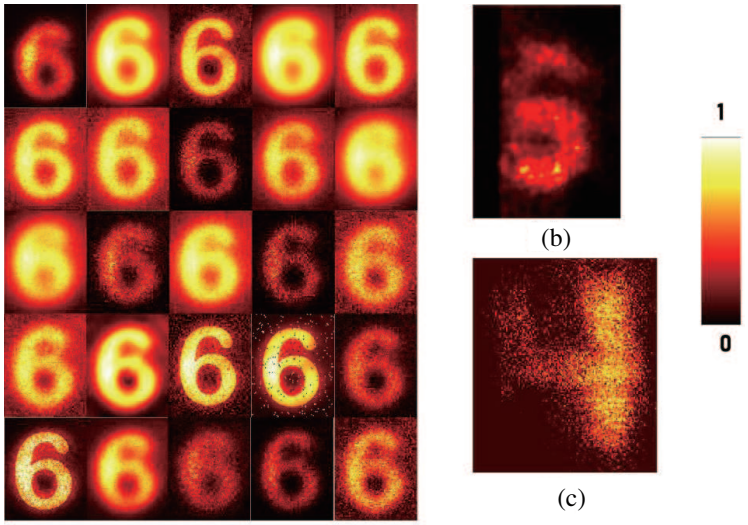

Figure 10: (a) Sample training set used for training the deep learning network. (b) noise removed image of number '6' by deep learning and (c) noise removed image of number '4' by edge enhancement.

5. CONCLUSION AND FUTURE PERSPECTIVES

In this study, a radical approach for developing a 3D imaging telescope called 3D-TELESCA is proposed. This approach has a significantly improved signal to noise ratio, light efficiency, and temporal resolution compared to PAIS and synthetic aperture approach developed based on I-COACH [4–7]. Even though the light efficiency of the proposed method is lower than conventional Cassegrain telescope, the 3D imaging capability and versatility can make this approach attractive and useful. The preliminary studies using a single sub-modulator realized by a QRL with a broad-band light source revealed valuable insights and the challenges lying ahead if this idea materialized. One major challenge is the chromatic aberrations of the diffractive elements which increased the background noise during reconstruction. It also means that correlation-based imaging can have only so many spatio-spectral channels. This is an important point which needs to be considered in the future design of coded aperture imagers. To achieve 3D imaging at different depths it seems necessary to suppress the spectral channels in the sensor by either reducing the chromatic aberrations or by using spectral filters. The above two solutions come with set of challenges on design and fabrication of coded apertures and loss of light power respectively. The two noise reduction approaches namely deep learning and contrast enhancement method improved the noisy results obtained from non-linear correlation. The deep learning results did not appear to vary significantly with the introduction of new noisy datasets. The contrast enhancement approach was tuned with different factors of the edge enhanced image and image obtained from non-linear correlation. In a way, both approaches consumed time. However, the deep learning approach was better as the time consumption was mostly offline, but the edge enhancement method required processing online. Further studies are required to find an optimal reconstruction method. The current experimental study did not use any statistical averaging and so there is a chance that the results will improve upon statistical averaging with multiple recordings. The current study was carried out with binary diffractive elements which an efficiency of around 36%. Future studies will involve high efficiency greyscale diffractive elements [20].

ACKNOWLEDGMENT

We acknowledge funding for the Nanolab by Swinburne University of Technology (SUT).
ARC LP190100505 is acknowledged for funding.

REFERENCES

1. Van der Avoort, C., S. F. Pereira, J. J. M. Braat, and J.-W. den Herder, "Optimum synthetic-aperture imaging of extended astronomical objects," *J. Opt. Soc. Am. A*, Vol. 24, No. 4, 1042–1052, 2007.

Authorized licensed use limited to: University of Tartu Estonia. Downloaded on June 20,2022 at 09:35:35 UTC from IEEE Xplore. Restrictions apply.

2. Karcı, O. and M. Ekinci, "Design of a high-precision, 0.5 m aperture Cassegrain collimator," *Appl. Opt.*, Vol. 59, No. 27, 8434–8442, 2020.
3. Goodman, J. W., *Introduction to Fourier Optics*, Roberts & Co. Publishers, Englewood, Colorado, 2005.
4. Bulbul, A., A. Vijayakumar, and J. Rosen, "Partial aperture imaging by systems with annular phase coded masks," *Opt. Express*, Vol. 25, No. 26, 33315–33329, 2017.
5. Bulbul, A., A. Vijayakumar, and J. Rosen, "Superresolution far-field imaging by coded phase reflectors distributed only along the boundary of synthetic apertures," *Optica*, Vol. 5, No. 12, 1607–1616, 2018.
6. Bulbul, A. and J. Rosen, "Super-resolution imaging by optical incoherent synthetic aperture with one channel at a time," *Photon. Res.*, Vol. 9, No. 7, 1172–1181, 2021.
7. Bulbul, A. and J. Rosen, "Partial aperture imaging system based on sparse point spread holograms and nonlinear cross-correlations," *Sci. Rep.*, Vol. 10, No. 1, 21983, 2020.
8. Vijayakumar, A. and J. Rosen, "Interferenceless coded aperture correlation holography — A new technique for recording incoherent digital holograms without two-wave interference," *Opt. Express*, Vol. 25, No. 12, 13883–13896, 2017.
9. Malinauskas, M., A. Žukauskas, S. Hasegawa, Y. Hayasaki, V. Mizeikis, R. Buividas, and S. Juodkazis, "Ultrafast laser processing of materials: From science to industry," *Light: Sci. Appl.*, vol. 5, No. 8, e16133, 2016.
10. Zhang, H. L., H. Liu, W. B. Xu, and Z. W. Lu, "Large aperture diffractive optical telescope: A review. *Opt. Laser Technol.*, Vol. 130, 106356, 2020.
11. Kim, D. W. and S. W. Kim, "Static tool influence function for fabrication simulation of hexagonal mirror segments for extremely large telescopes," *Opt. Express*, Vol. 13, No. 3, 910–917, 2005.
12. Gerchberg, R. W. and W. O. Saxton, "A practical algorithm for the determination of phase from image and diffraction plane pictures," *Optik*, Vol. 35, 227–246, 1972.
13. Vijayakumar, A., Y. Kashter, R. Kelner, and J. Rosen, "Coded aperture correlation holography system with improved performance [Invited]," *Appl. Opt.*, Vol. 56, No. 13, F67–F77, 2017.
14. Rosen, J. and G. Brooker, "Digital spatially incoherent Fresnel holography," *Opt. Lett.*, Vol. 32, No. 8, 912–914, 2007.
15. Bouchal, P. and Z. Bouchal, "Selective edge enhancement in three-dimensional vortex imaging with incoherent light," *Opt. Lett.*, Vol. 37, No. 14, 2949–2951, 2012.
16. Anand, V., T. Katkus, S. H. Ng, and S. Juodkazis, "Review of Fresnel incoherent correlation holography with linear and non-linear correlations [Invited]," *Chin. Opt. Lett.*, Vol. 19, No. 2, 020501-, 2021.
17. Anand, V., J. Rosen, S. H. Ng, T. Katkus, D. P. Linklater, E. P. Ivanova, and S. Juodkazis, "Edge and contrast enhancement using spatially incoherent correlation holography techniques," *Photonics*, Vol. 8, No. 6, 224, 2021.
18. Anand, V., S. N. Ng, T. Katkus, and S. Juodkazis, "White light three-dimensional imaging using a quasi-random lens," *Opt. Express*, Vol. 29, No. 10, 15551–15563, 2021.
19. Rai, M. R., A. Vijayakumar, and J. Rosen, "Non-linear adaptive three-dimensional imaging with interferenceless coded aperture correlation holography (I-COACH)," *Opt. Express*, Vol. 26, No. 14, 18143–18154, 2018.
20. Jonušauskas, L., D. Gailevičius, S. Rekštytė T. Baldacchini, S. Juodkazis, and M. Malinauskas, "Mesoscale laser 3D printing," *Opt. Express*, Vol. 27, No. 11, 15205–15221, 2019.

Authorized licensed use limited to: University of Tartu Estonia. Downloaded on June 20,2022 at 09:35:35 UTC from IEEE Xplore. Restrictions apply.
View publication stats